

## Local Pair Correlations in One-Dimensional Bose Gases

Toshiya Kinoshita, Trevor Wenger, and David S. Weiss

*Department of Physics, The Pennsylvania State University, 104 Davey Lab, University Park, Pennsylvania, 16802 USA*

(Received 14 July 2005; published 3 November 2005)

We measure photoassociation rates in one-dimensional Bose gases, and so determine the local pair correlation function over a wide range of coupling strengths. As bosons become more strongly coupled, we observe a tenfold decrease in their wave function overlap, thus directly observing the fermionization of bosons.

DOI: [10.1103/PhysRevLett.95.190406](https://doi.org/10.1103/PhysRevLett.95.190406)

PACS numbers: 03.75.Hh, 05.30.Jp, 32.80.Pj, 68.65.-k

Ultracold atoms in optical lattices are well controlled many-body physical systems [1]. Theoretical models that are intractable on classical computers can be designed directly into an experiment, and the solutions can be measured. Coupled spin systems [2–4],  $d$ -wave paired superconductors [5], and new quantum phases [6] are among the problems that could be solved in this way. One-dimensional (1D) Bose gases are ideal test beds for this approach, since they are among the few many-body systems that can be exactly solved theoretically [7–9]. One can even derive properties that are notoriously difficult to calculate in strongly coupled systems, like the local pair correlation,  $g^{(2)}$  [10], which is proportional to the probability of observing two particles in the same place. In this Letter, we present a measurement of  $g^{(2)}$  for 1D Bose gases across a 30-fold range of coupling strength. There is an order of magnitude reduction in  $g^{(2)}$  for the strongest coupling, and excellent agreement with theory over the whole range.

1D Bose gases are typically parametrized by the universal coupling constant  $\gamma$  [7]. The behavior of 1D Bose gases in different coupling regimes is readily characterized by the local pair correlation,  $g^{(2)} = \langle \Psi(z')^\dagger \Psi(z')^2 \rangle / n_{1D}^2$ , where  $\Psi(z')$  is the atom field operator and  $n_{1D} = \langle \Psi(z')^\dagger \times \Psi(z') \rangle$  is the 1D linear density [10]. A dense, weakly interacting 1D Bose gas ( $\gamma \ll 1$ ) is described well by mean-field theory. Its  $g^{(2)}$  is close to 1, just as in a 3D Bose-Einstein condensate (BEC). A dilute, strongly interacting 1D Bose gas ( $\gamma \gg 1$ ) is a Tonks-Girardeau (TG) gas. Its  $g^{(2)}$  approaches zero, just like a gas of noninteracting 1D fermions. The strong coupling limit, where theory is difficult in more than 1D, is especially important in condensed matter physics. Atomic Bose gases have only attained strong coupling in Mott insulator states [11] and in 1D [12,13]. Previous 1D experimental results in the intermediate coupling [14–16] and TG regimes [12,13] have been in accord with the exact 1D Bose gas theory [7,17]. But these results have relied on mostly indirect manifestations of strong coupling. In contrast,  $g^{(2)}$  directly reveals the extent of wave function overlap.

Large correlations among bosonic wave functions in 1D act in a way that is mathematically analogous to Pauli exclusion for fermions [7,9]. As for fermions, strongly

coupled 1D boson wave functions have little overlap on distance scales that are small compared to the wave functions [10]. This small scale can still be much larger than the Å range in which electron clouds repel each other, where no atoms in any dimension can have significant wave function overlap. Our measurements of  $g^{(2)}$  are carried out at such (nanometer scale) separations.

We start the experiment with a nearly (95%) pure  $^{87}\text{Rb}$  BEC of  $2.5\text{--}3 \times 10^5$  atoms in the lowest energy state  $F = m_F = 1$ , produced in a compressible crossed dipole force trap (made with  $1.06 \mu\text{m}$  light) and a levitating magnetic field [18]. 1D Bose gases are created by adiabatically superimposing a  $600 \mu\text{m}$  waist, blue-detuned 2D optical lattice on the crossed dipole trap [see Fig. 1(a)]. This yields arrays of  $\sim 1000\text{--}8000$  parallel, nearly identical, 1D traps, depending on the power per crossed dipole beam,  $P_{\text{cd}}$ . The number of atoms per tube,  $N_{\text{tube}}$ , is on average between 40 and 240 [13]. Atoms in these traps are 1D because the lowest transverse vibrational excited state is well above all other dynamical energy scales. The atomic wave functions have transverse extent, but since the transverse wave functions do not change during the experiment, the dynamics are purely 1D. The crossed dipole trap, with its beam waist adjusted to  $120 \mu\text{m}$ , provides variable harmonic confinement along the 1D tubes created by the 2D optical lattice. In all experimental runs, the final depth of the 2D lattice potential exceeds  $30E_{\text{rec}}$ , so that tunneling among tubes is negligible [13].

For atoms confined in 1D, the interaction strength is described by

$$\gamma \approx \frac{2a}{n_{1D}a_r^2} \quad (1)$$

(as long as  $a \ll a_r$ ), where  $n_{1D}$  is the linear density,  $a$  is the (3D) positive scattering length ( $a = 5.3 \text{ nm}$  for our atoms), and  $a_r = (\hbar/m\omega_r)^{1/2}$  is the transverse extent of the atomic wave function ( $a_r \geq 35 \text{ nm}$  in our measurements), where  $m$  is the atomic mass and  $\omega_r$  is the transverse oscillation frequency [19]. By changing the optical lattice depth, we change  $a_r$ , and by changing  $P_{\text{cd}}$ , we change  $n_{1D}$  [13]. Specifically, high  $P_{\text{cd}}$  leads to high  $n_{1D}$ , both because the high initial BEC density leads to more atoms per tube in the 2D lattice, and because those atoms are more compressed

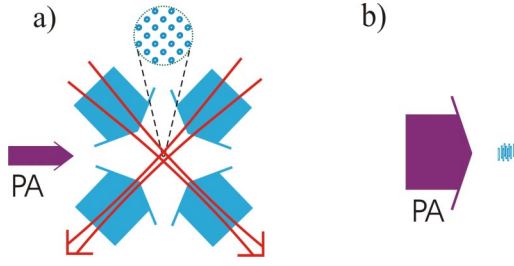


FIG. 1 (color online). Experimental geometry. (a) Laser beam configuration, top view. Four blue-detuned beams with  $600 \mu\text{m}$  waists, shown as fat arrows incident from the corners of the frame, create a 2D optical lattice with  $390 \text{ nm}$  lattice constant. The 2D lattice is superimposed on a pair of  $120 \mu\text{m}$  waist, red-detuned laser beams that form a crossed dipole trap. The combination of these beams creates a trapped array of parallel 1D Bose gases, as illustrated in the circular blow-up of the central region. The  $280 \mu\text{m}$  waist photoassociation beam (labeled PA), uniformly illuminates all the 1D Bose gases. (b) Trapped atom distribution, side view. The atoms are confined radially in the vibrational ground state, with characteristic radii that range from  $35$  to  $50 \text{ nm}$ . The full axial lengths of the atom clouds range from  $15$  to  $50 \mu\text{m}$ , much smaller than the photoassociation beam. There are thousands of independent 1D Bose gases. Aspect ratios range from  $\sim 150$  to  $700$ .

in 1D. As  $P_{\text{cd}}$  is varied from  $36 \text{ mW}$  to  $3.1 \text{ W}$ , the 3D Thomas-Fermi radius ranges from  $20 \mu\text{m}$  to  $8.2 \mu\text{m}$ ,  $N_{\text{tube}}$  for the central tubes ranges from  $65$  to  $390$ , and the axial oscillation frequency,  $\omega_z/2\pi$ , ranges from  $15 \text{ Hz}$  to  $150 \text{ Hz}$ . In this way, we can vary  $\gamma$  from  $0.37$  to  $11$ , reaching a factor of 2 stronger coupling than has previously been achieved for a freely moving 1D Bose gas [13].

The maximum spontaneous emission rates are  $0.4 \text{ s}^{-1}$  due to the lattice light, which is detuned from the D2-line resonance by  $3.2 \text{ THz}$ , and  $0.28 \text{ s}^{-1}$  due to the crossed dipole light. We measure that nonadiabatic heating due to the lattice being turned on is minimal [13]. Because the heating that results from spontaneous emission is less severe when the 1D density is lower, we can decrease the lattice detuning to  $1.6 \text{ THz}$  for the smallest density.

Atomic local [20–23] and nonlocal [24,25] pair correlations have previously been measured in contexts other than 1D Bose gases. In our 1D Bose gases, we measure  $g^{(2)}$  by photoassociation, using light resonant with the molecular state  $|0^-_g(\sim S_{1/2} + P_{3/2}), \nu = 1, J = 2\rangle$ , located  $\sim 26.7 \text{ cm}^{-1}$  below the D2 line, where  $\nu$  and  $J$  are the vibrational and rotational quantum numbers, respectively [26]. Under our experimental conditions, the stimulated transition rate between the continuum ground state and the bound molecular state,  $\Gamma_{\text{stim}}$ , is much less than the spontaneous decay rate of the molecule,  $\Gamma_{\text{spon}} (\sim 2\pi \times 12 \text{ MHz})$ . The photoassociation rate,  $K_{3\text{D}}$ , can be calculated by two-body  $s$ -wave scattering theory [27]. For a pure 3D BEC,

$$K_{3\text{D}} = \frac{8\pi\hbar}{mk} \frac{\Gamma_{\text{stim}}}{\Gamma_{\text{spon}}}$$

where  $\hbar k$  is the relative momentum of the two particles. For

the small  $k$ 's that prevail in ultracold atom experiments,  $\Gamma_{\text{stim}}$  is proportional to  $k$ , making  $K_{3\text{D}}$  velocity independent [27]. Photoassociation is most likely to occur at very short interparticle distances, between  $1.6$  and  $1.9 \text{ nm}$  [28]. This distance scale is much less than the typical extent of the trapped atom wave functions, either in 1D ( $> \sim 300 \text{ nm}$ ) or transversely ( $> 35 \text{ nm}$ ). Therefore the photoassociation rate in 1D is proportional to the 3D photoassociation rate, but reduced by the loss of wave function overlap due to the atoms being confined to 1D,

$$K_{1\text{D}} = K_{3\text{D}}g^{(2)}. \quad (2)$$

The  $60 \text{ mW}$ ,  $280 \mu\text{m}$  waist photoassociation beam is locked to a Fabry-Perot cavity that is, in turn, locked to the  $^{87}\text{Rb}$  D2 resonance, giving a linewidth below  $2 \text{ MHz}$ , smaller than the measured  $13 \text{ MHz}$  linewidth of the photoassociation spectrum. The beam is linearly polarized perpendicular to the  $7 \text{ Gauss}$  bias magnetic field and propagates in the horizontal plane of the 2D lattice. It is much larger than the trapped atom region [see Fig. 1(b)]. The photoassociation beam is pulsed on for between  $25 \mu\text{s}$  and  $1 \text{ ms}$ , which is at most  $1/65$  of the axial oscillation period. The pulse is short enough that there is negligible axial redistribution of atoms, either due to loss of atoms or the photoassociation beam's dipole force. The rate that photoassociation light is scattered from the D2 line is  $8 \text{ s}^{-1}$ , and can be neglected.

Immediately after photoassociation, we shut off all trapping potentials and take a high intensity fluorescence image [29] to determine the number of remaining atoms,  $N_{r\text{PA}}$ . Sixteen images are averaged for each data point. When the photoassociation pulse is  $700 \text{ MHz}$  from the molecular resonance, the number of the atoms left,  $N_{or\text{PA}}$ , is similarly measured. The off-resonant photoassociation pulse causes less than  $1\%$  loss. The measured fractional loss due to photoassociation,  $f$ , is given by  $f = (N_{or\text{PA}} - N_{r\text{PA}})/N_{or\text{PA}}$ .

Figure 2 shows  $f$  as a function of the photoassociation time,  $T_{\text{PA}}$ , for two illustrative trap conditions. The solid curves are fits of the shorter time data to the solution of a two-body loss equation. For the rest of the data in this Letter, we use  $T_{\text{PA}}$ 's that keep  $f$  less than  $0.15$ , so that the loss rate is approximately constant. In this way, we experimentally determine the fractional photoassociation loss rate,  $\Gamma_L = -\frac{1}{N} \frac{dN}{dt} = f/T_{\text{PA}}$ .

We collect data in sets characterized by the initial 3D BEC density, which we vary from  $3.2 \times 10^{13} \text{ cm}^{-3}$  to  $4.1 \times 10^{14} \text{ cm}^{-3}$  by adjusting  $P_{\text{cd}}$ . At each initial density, we measure  $\Gamma_L$  both in the 3D BEC and for a range of optical lattice depths, i.e., of transverse confinement in 1D tubes. In Fig. 3, for each set, we plot the ratio of  $\Gamma_L$  normalized to the 3D BEC value of  $\Gamma_L$  as a function of the optical lattice depth, in units of the recoil energy,  $E_{\text{rec}}$ .

Figure 3 demonstrates the decrease in  $g^{(2)}$  with increasing  $\gamma$  in two ways. Within each curve the axial confinement is fixed, as is the number of atoms in each tube. The

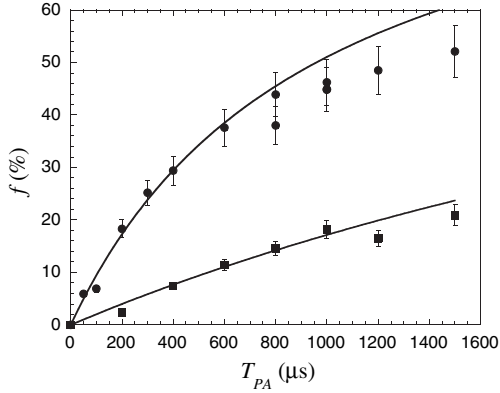


FIG. 2. Atom loss by photoassociation. The fractional loss is plotted as a function of the photoassociation time. The circles (squares) correspond to  $P_{\text{cd}} = 320$  mW (36 mW). The solid curves are fits to a theory that assumes that  $dN/dt$  is proportional to  $N^2$  up to 600  $\mu\text{s}$  (800  $\mu\text{s}$ ) for 320 mW (36 mW). The error bars reflect measured statistical fluctuations.

individual curves show that  $\Gamma_L$  only weakly depends on the lattice depth, even though the atoms become more tightly confined as the lattice depth is increased. The results are most striking when we compare the curves from top to bottom. For the top curve, which corresponds to high initial density ( $n_{3\text{D}} = 4.1 \times 10^{14} \text{ cm}^{-3}$ ), turning on the 2D lattice increases the loss by as much as a factor of 2.8. The extra loss can be qualitatively understood because the lattice confines the atoms in a smaller volume. But the increased losses get progressively smaller for lower initial

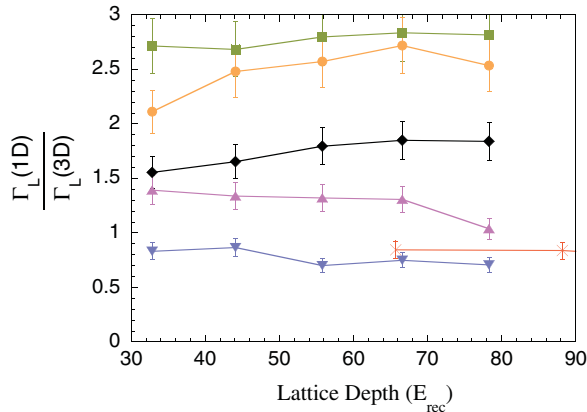


FIG. 3 (color online). The effect of 1D confinement on photoassociative loss. The ratio of loss in 1D to loss in 3D is shown as a function of the 2D lattice depth. The error bars are standard deviations that characterize fluctuations in the total number of the atoms (which are  $\sim 10\%$ ). The different curves correspond to different crossed dipole trap powers, and hence different  $n_{1\text{D}}$ . In order from higher to lower density, and from top to bottom on the graph: squares,  $P_{\text{cd}} = 3.1$  W; circles,  $P_{\text{cd}} = 1$  W; diamonds,  $P_{\text{cd}} = 320$  mW; up triangles,  $P_{\text{cd}} = 110$  mW; and down triangles,  $P_{\text{cd}} = 36$  mW. The crosses correspond to  $P_{\text{cd}} = 36$  mW, but with a lattice detuning of 1.6 THz instead of 3.2 THz, and the larger  $E_{\text{rec}}$  points are omitted. The solid lines are to guide the eye.

densities, until by the lowest two curves (for which the initial density is  $n_{3\text{D}} = 3.2 \times 10^{13} \text{ cm}^{-3}$ ), turning on the lattice actually *decreases*  $\Gamma_L$ . That is, we reach a regime where the reduction of  $g^{(2)}$  associated with being in 1D is greater than the local density enhancement due to the 1D confinement.

To quantitatively compare our measurements with the exact 1D Bose theory for  $g^{(2)}(\gamma)$  [10], we need to apply the theory to our ensemble of atoms, each of which experiences a different local density, and hence a different  $\gamma$ . Since, as we shall see,  $g^{(2)}$  varies roughly linearly with  $\log(\gamma)$  over the range of  $\gamma$  used in our experiment, we define  $\gamma_{\text{eff}}$  for an ensemble of atoms so that  $\log(\gamma_{\text{eff}})$  is the weighted average of  $\log(\gamma)$ . As we show below, experimental values for  $g^{(2)}(\gamma_{\text{eff}})$  can then be calculated without reference to the 1D theory. Each tube sees nearly identical trap light, but  $N_{\text{tube}}$  is tube dependent. Within a given tube,  $n_{1\text{D}}(z) = N_{\text{tube}}s(z)$ , where  $s(z)$  is a distribution function that depends on  $N_{\text{tube}}$  and the trap details, and can be numerically calculated using the results in Ref. [17]. Such calculations and Eq. (1) allow us to calculate  $\gamma_{\text{eff}}$  for each tube, and then for the ensemble of tubes.

As for any two-body loss process, the governing equation for  $\Gamma_L$  within a tube is

$$\Gamma_L = \frac{2K_{3\text{D}}}{N} \int n_{3\text{D}}(r)^2 g^{(2)}(z) dV, \quad (3)$$

where we have used Eq. (2).  $n_{3\text{D}}$  within each tube depends on  $n_{1\text{D}}$  and the 2D harmonic oscillator ground state wave function,

$$n_{3\text{D}}(\rho, z) = \frac{n_{1\text{D}}(z)}{\pi a_r^2} \exp\left(-\frac{\rho^2}{a_r^2}\right). \quad (4)$$

If we replace  $g^{(2)}(z)$  by  $g^{(2)}(\gamma_{\text{eff}})$ , we can pull it out of the integral in Eq. (3) so that

$$g^{(2)}(\gamma_{\text{eff}}) = \frac{\Gamma_L}{2K_{3\text{D}}\langle n_{3\text{D}} \rangle}. \quad (5)$$

We calculate  $\langle n_{3\text{D}} \rangle$  by averaging  $n_{3\text{D}}(\rho, z)$  within each tube and then over all the tubes. To do so, we assume that the atoms are distributed among tubes according to a Thomas-Fermi distribution with the length scale associated with the source 3D BEC. This is only a rough and convenient approximation to the actual distribution when a 3D Thomas-Fermi profile is projected onto tubes. The actual distribution can change as a result of tunneling among tubes during the adiabatic turn-on of the lattice. Our experimental knowledge of the exact distribution is limited by the spatial resolution of our imaging. To address this uncertainty, we repeat our calculations with other distribution functions, and find both  $\gamma_{\text{eff}}$  and  $n_{3\text{D}}$  to be quite insensitive to the exact distribution among tubes. For example,  $\gamma_{\text{eff}}$  and  $n_{3\text{D}}$  each change by less than 5% if we assume a flattop distribution among the tubes with the measured rms width and the same total number of atoms.

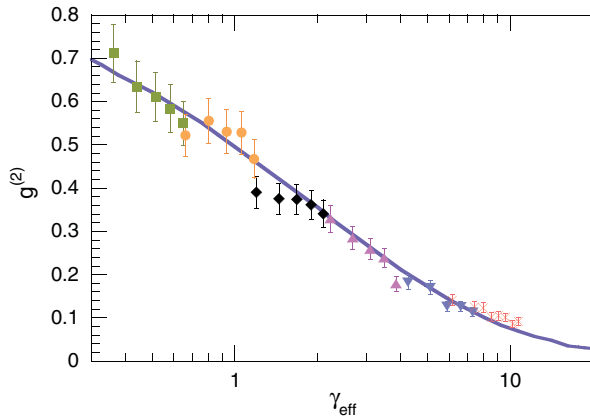


FIG. 4 (color online). The local pair correlation function vs the coupling strength. The solid blue line is the 1D Bose gas theory [10]. The points and associated error bars are generated from the same data used in Fig. 3. Here,  $g^{(2)}$  is calculated for each point and the points are arranged according to the coupling parameter  $\gamma_{\text{eff}}$ . The data labels correspond to those in Fig. 3. A scale factor proportional to  $K_{3D}$  has been determined by a weighted least squares fit of the data to the theory. This value of  $K_{3D}$  accords with our direct measurement of  $K_{3D}$  using 3D BECs.

The solid curve in Fig. 4 is the result of the zero temperature 1D Bose gas theory for  $g^{(2)}(\gamma)$  [10]. We use Eqs. (4) and (5) to plot the data from Fig. 3 (with corresponding labels) in Fig. 4.  $K_{3D}$  is left as a free parameter, so that it acts as a scaling factor for the data. A weighted least squares fit to the theory determines  $K_{3D} = 4.3 \times 10^{-10} \text{ cm}^3/\text{s}$ . Over our measured range between  $\gamma_{\text{eff}} = 0.37$  and 11,  $g^{(2)}(\gamma_{\text{eff}})$  varies by an order of magnitude. The agreement between theory and experiment is excellent over the whole range of  $\gamma_{\text{eff}}$ . In the weak coupling limit,  $g^{(2)}$  approaches one, like a 3D BEC. Strong coupling makes  $g^{(2)}$  approach zero, showing that strongly interacting bosons act like fermions.

Our experiment provides a more direct way to measure  $K_{3D}$ , using the  $\Gamma_L$  results for the 3D BECs, and Eq. (5) with  $g^{(2)}$  set equal to 1. Averaging these results, we determine  $K_{3D} = 4.7 \times 10^{-10} \text{ cm}^3/\text{s}$ , with a statistical standard deviation ( $\sigma_{K_{\text{st}}}$ ) of  $0.3 \times 10^{-10} \text{ cm}^3/\text{s}$ . The systematic uncertainty in this measurement of  $K_{3D}$  is  $0.6 \times 10^{-10} \text{ cm}^3/\text{s}$ , larger than  $\sigma_{K_{\text{st}}}$ , primarily due to our  $\pm 5 \text{ }\mu\text{m}$  uncertainty in the crossed dipole beam waist, which affects  $\langle n_{3D} \rangle$  in Eq. (4).

We can compare the direct measurement of  $K_{3D}$  to the value determined from Fig. 4 in order to test the 1D Bose theory without any free parameters. Because the systematic uncertainty in the direct measurement of  $K_{3D}$  is highly correlated with the systematic uncertainty in  $\langle n_{3D} \rangle$  for the 1D Bose gas, the systematic uncertainty in the scale for  $g^{(2)}(\gamma_{\text{eff}})$  turns out to be less than 1% ( $0.1 \times \sigma_{K_{\text{st}}}/K_{3D}$ ). The no free parameter test is thus quite robust against systematic errors. The two separate determinations of  $K_{3D}$  agree to within 9%, or  $1.3 \times \sigma_{K_{\text{st}}}$ . We have thus tested the 1D Bose theory to within this uncertainty.

In conclusion, we have created a 1D Bose gas, which is a rare example of an exactly theoretically solvable many-body system. The central result of the solutions, that bosonic wave functions overlap progressively less as the strength of their interactions is increased, is quantitatively confirmed in the experiment. The specific technique used here could also be used to study pair correlations at non-zero temperatures [30], in 2D Bose gases [31], and in a wide variety of lattice gases. The success of the experiment presented here suggests that similar experiments might be used to find the solutions of previously unsolvable many-body models [2–6].

We acknowledge discussions with Ken O’Hara and Kurt Gibble, and financial support from the National Science Foundation, Grant No. PHY-0457206.

- 
- [1] D. Jaksch and P. Zoller, *Ann. Phys. (N.Y.)* **315**, 52 (2005).
  - [2] A. Sørensen and K. Mølmer, *Phys. Rev. Lett.* **83**, 2274 (1999).
  - [3] J. Garcia-Ripoll, M. Martin-Delgado, and J. Cirac, *Phys. Rev. Lett.* **93**, 250405 (2004).
  - [4] L.-M. Duan, E. Demler, and M. Lukin, *Phys. Rev. Lett.* **91**, 090402 (2003).
  - [5] W. Hofstetter *et al.*, *Phys. Rev. Lett.* **89**, 220407 (2002).
  - [6] E. Demler and F. Zhou, *Phys. Rev. Lett.* **88**, 163001 (2002).
  - [7] E. H. Lieb and W. Liniger, *Phys. Rev.* **130**, 1605 (1963).
  - [8] C. N. Yang and C. P. Yang, *J. Math. Phys. (N.Y.)* **10**, 1115 (1969).
  - [9] M. Girardeau, *J. Math. Phys. (N.Y.)* **1**, 516 (1960).
  - [10] D. Gangardt and G. Shlyapnikov, *Phys. Rev. Lett.* **90**, 010401 (2003).
  - [11] M. Greiner *et al.*, *Nature (London)* **415**, 39 (2002).
  - [12] B. Paredes *et al.*, *Nature (London)* **429**, 277 (2004).
  - [13] T. Kinoshita, T. Wenger, and D. S. Weiss, *Science* **305**, 1125 (2004).
  - [14] H. Moritz *et al.*, *Phys. Rev. Lett.* **91**, 250402 (2003).
  - [15] T. Stöferle *et al.*, *Phys. Rev. Lett.* **92**, 130403 (2004).
  - [16] B. Laburthe-Tolra *et al.*, *Phys. Rev. Lett.* **92**, 190401 (2004).
  - [17] V. Dunjko, V. Lorent, and M. Olshanii, *Phys. Rev. Lett.* **86**, 5413 (2001).
  - [18] T. Kinoshita, T. Wenger, and D. S. Weiss, *Phys. Rev. A* **71**, 011602(R) (2005).
  - [19] M. Olshanii, *Phys. Rev. Lett.* **81**, 938 (1998).
  - [20] M. Yasuda and F. Shimizu, *Phys. Rev. Lett.* **77**, 3090 (1996).
  - [21] W. Ketterle and H.-J. Miesner, *Phys. Rev. A* **56**, 3291 (1997).
  - [22] C. McKenzie *et al.*, *Phys. Rev. Lett.* **88**, 120403 (2002).
  - [23] G. B. Partridge *et al.*, *cond-mat/0505353*.
  - [24] M. Greiner *et al.*, *Phys. Rev. Lett.* **94**, 110401 (2005).
  - [25] S. Fölling *et al.*, *Nature (London)* **434**, 481 (2005).
  - [26] M. Theis *et al.*, *Phys. Rev. Lett.* **93**, 123001 (2004).
  - [27] J. L. Bohn and P. S. Julienne, *Phys. Rev. A* **56**, 1486 (1997).
  - [28] A. Fioretti *et al.*, *Eur. Phys. J. D* **15**, 189 (2001).
  - [29] M. T. DePue *et al.*, *Opt. Commun.* **180**, 73 (2000).
  - [30] K. V. Kheruntsyan *et al.*, *Phys. Rev. Lett.* **91**, 040403 (2003).
  - [31] D. Rychtarik *et al.*, *Phys. Rev. Lett.* **92**, 173003 (2004).